STATIC AND FATIGUE PROPERTIES OF 3D PRINTED CONTINUOUS CARBON FIBER NYLON COMPOSITES

Efstratios Giannakis[1], Christos Koidis[1], Panagiotis Kyratsis[2], Dimitrios Tzetzis[1]

[1]International Hellenic University, School of Science and Technology, 14th km Thessaloniki – N. Moudania, GR57001,Thermi, Greece
[2]Western Macedonia University of Applied Sciences, Department of Mechanical Engineering and Industrial Design, GR50100, Kila Kozani, Greece

Corresponding author: Dimitrios Tzetzis, d.tzetzis@ihu.edu.gr

Abstract: CFRPs provide excellent mechanical properties and tailor-made designs for several applications. Using continuous fiber fabrication (CFF) 3D printing technology, 3D printed constructs with mechanical properties higher than common 3D printed components can be printed. However, challenges remain such as the standardization of processes and characterization techniques to ensure the production of 3D printed CFRPs with good consolidation of reinforcement fibers into the polymer matrix and controlled fiber orientation. In this work, 3D printed carbon fiber nylon mechanical properties are investigated through static tensile and fatigue tests in order to assess the performance of such structures. Also, the mechanical properties of 3D printed PLA and nylonareexaminedfor comparison. As expected, the results areshown that the pure nylon specimens had plastic deformation behaviour (as it was also for PLA) in contrast to carbon fiber reinforced nylon, which had almost elastic deformation behaviour. The modulus and strength were significantly increased. The fatigue results (R=0) showed that the carbon fibres are relatively insensitive to such a loading regime.

Key words: 3D printing, carbon fiber, nylon, fatigue, continuous filament fabrication, mechanical properties.

1. INTRODUCTION

3D printing is at the forefront of research activities worldwide, as the commercial exploitation of this technology is expected to displace some traditional manufacturing methods over the next few years [1-2]. 3D print materials currently available on the market have limited mechanical properties, thereby it is necessary to develop printable materials for special applications with high performance [3-8]. Composite materials can be printed using the Fused Deposition Modelling (FDM) 3D printing technique where a thermoplastic material is extruded through a hot nozzle. The viscous material solidifies on the build plate forming parts with accuracy typically in the order of 100μm. The mechanical properties of 3D printed parts can deviate significantly from the material bulk properties due to the structure formed on the meso-scale during printing [9].

During processing, parameters such as temperature, viscosity and surface energy play an important role in material flow properties and more importantly, how the final interface between the beads is formed. Furthermore, the effect of raster angle can lead to different properties across the principal material directions [10], like the orthotropic behaviour of fibre composites, with diminished mechanical properties of the printed parts [11].

Important features that strongly affect the mesostructure (arrangement of material(s) within the component) and the mechanical properties of the component are the contact area between the printed lines and the minimization of the overall void content by optimizing the printing process. This process is sensitive to the viscosity (temperature dependent), thermal conductivity and heat capacity of the material, as well as the cooling rate (determined by external environment) [12].

The FDM process can also be used to print carbon fiber reinforced plastics (CFRPs) by adding fibres into the thermoplastic filament [13, 14]. CFRPs provide excellent mechanical properties and tailor-made designs for several applications [11, 12]. Morever, they provide stability to the parts, reducing and even avoiding the shape distortions that usually appear in the printing of 3D parts [15]. However, challenges remain such as the processes to ensure the production of CFRPs with good consolidation of reinforcement fibers into the polymer matrix, controlled fiber orientation and low cost. While a wide range of CFRPs are available for the manufacturing of composites, most of them are produced in a two-stage process during which pressure needs to be applied over the entire part surface area, which requires expensive equipment leading to increased production costs. Using Continuous Filament Fabrication (CFF) technology developed by Markforged [16], continuous fiber reinforced polymers with mechanical properties higher than common 3D printers can be printed. This opens new applications in both personal fabrication market and manufacturing of

lightweight parts for industry. During processing using this printer, first, a matrix of nylon oronyxis constructed and then matrix is overlayedwithfiber filament layer by layer. Patterning is important, because it changesthe structure of the component. Both micro- and macro-structurearecritical for the mechanical properties and performance of the parts. In view of this, the mechanical characterization of the materials is crucial to optimize materials and properties and produce cost-efficient industrial parts.

Fatigue is one of the most important properties since it is the process of progressive localized permanent structural change occurring in a material subjected to conditions that produce fluctuating stresses and strains at some point or points that may culminate in cracks or complete fracture after a sufficient number of fluctuations [17]. During fatigue, parts fail due to usage without reaching their static limit. Fatigue includes several processes such as the various defects and pores created during the solidification and their effect on the fracture and (fatigue) resistance. In this light, during 3D printing the entrainment of voids during solidification becomes a key issue to optimize materials and processes.

About (50–90)% of mechanical failures are related to fatigue [18]. However, since CFF is a newly developed technology, not many of the properties have been investigated yet and relatively little experimental data is available [19-23]. In this work, 3D printed specimens of carbon fiber nylon are assessedthrough tensile and fatigue tests aiming at adding to the knowledge base critical information on material's mechanical response. Carbon fiber nylon with advanced mechanical properties was efficiently fabricated using the established 3D printing CFF technology (double extruder with two nozzles, one for the matrix made of nylon, and one for the continuous carbon fibers) and by optimizing the 3D printing process. Also, 3D printed polylactic acid (PLA) and polyamide (nylon) are examined in comparison to carbon fiber nylon.

2. MATERIALS AND METHODS

Tensile tests were performed according to Standard Test Method for Tensile Properties of Polymer Matrix Composite Materials, ASTM D3039/D3039M – 14 [24]. The tensile test machine used for these tests was a Testometric M500-50 AT with a load cell of 50kN and a clamping device. In accordance with ASTM the head speed was set at 2mm/min and displacement and force was recorded to the test rig's data acquisition and control unit.

PLA samples were printed using a sigma BCN3D 3D printer. The printer has an extruder that deposits molten material with a nozzle on a building plate layer by layer. Stepper motors are used to move the extruder and/or the table in the three axes.

The PLA specimens, shown in Figure1, were fabricated with a layer thickness of 0.125mm. This allows only unidirectional structure in the central area of interest, at 0 deg, which, according to the preliminary comparison tests performed, was the strongest configuration.

Fig. 1. PLA tension specimens, 3D printed according to ASTM D3039/D3039M – 14 [23]

Nylon and nylon-carbon samples were printed using a Markforged Mark Two CFF printer. The system uses the FDM technology together with laying continuous fibers, for this reason it features a double extruder with two nozzles, one for the matrix, made of nylon, and one for the continuous fibers (carbon, fiberglass, Kevlar or HSHT glass) [16].

The nylon specimens, shown in Figure 2, were fabricatedalso with a layer thickness of 0.125mm to allow only unidirectional structure in the central area of interest, at 0 deg.

Fig. 2. Nylon tension specimens 3D printed according to ASTM D3039/D3039M – 14 [24]

The nylon-carbon specimens, shown in Figure 3, were fabricated horizontally as well, with a layer thickness of 0.125mm. The layers were adjusted to have the carbon fibres along the specimens, at 0deg, limiting the formation of a notch that could negatively affect specimen's strength. The pattern used was the isotropic fibre pattern for best layup configuration for tensile stresses, as it is shown in Figure 4. An example of the layup sequence can be seen in Figure 5. In addition, isotropic infill carbon fiber has shown higher resistance to fatigue failure in comparison to concentric [23]. The concentric pattern, which traces a specific number of shells within the outside contours of the part, helps to reinforce from bending around the z axis [16].

Fig. 3. Nylon-carbon tension specimens 3D printed according to ASTM D3039/D3039M – 14 [24]

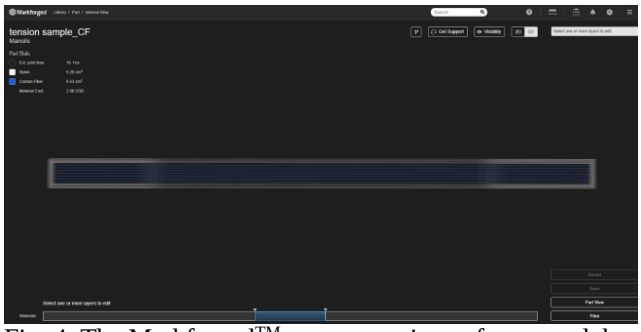

Fig. 4. The Markforged™ pre-processing software and the tensile specimen with the isotropic fiber pattern

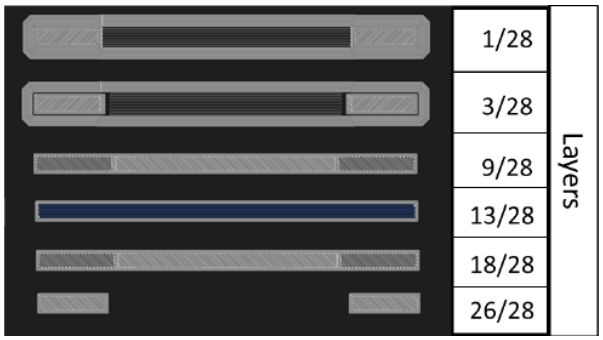

Fig. 5. Example of the layer setup

Additionally, tests were performed to examine whether the FDM method produces orthotropic parts. Therefore, extra PLA specimens were fabricated. These specimens (labelled as PLA-v), were built vertically (with a length of 10mm), in order to test the adhesion of the layers in tension with a layer thickness of 0.2mm. Building up the samples vertically allows only unidirectional structure in the central critical area, at 90 deg. Figure 6 shows how the specimen was placed on the printing bed.

Fig. 6. Vertical building of the PLA sample on the printing bed

In Table 1, the dimensions of all specimens are collected for comparison, where l is the length, w is the width, t is the thickness and A is the cross-section surface area of the specimens. The nylon-carbon's A value refers to the carbon cross section area only, due to the great difference between the mechanical characteristics of nylon and carbon components [19].

Table 1.Specimen dimensions

Specimen	l (mm)	w (mm)	t (mm)	A (mm^2)
Nominal	100	10.00	1.50	15.00
PLA-v	10	9.87	1.45	14.31
PLA	100	10.07	1.68	16.91
Nylon	100	10.07	1.68	16.10
Nylon-carbon	100	6.50	0.60	3.90

The configuration for fatigue experiments of nylon-carbon samples includes a strain gage attached on the samples (Figure 7), as the fatigue tests have to be strain controlled. A grinder with high grinding velocity was used to configure heat transfer surfaces and control their roughness. The specimens were clamped to the test rig and after a quick check of the specimens' stiffness and stresses in different loadings (lower than the actual test), the control unit drove the actuator to move up and down controlling the forces. The forces were set to reach the wanted stress amplitude and mean stresses.

Fig. 7. CFF carbon-nylon fatigue specimens

The frequency of the tests was set to a maximum of 2Hz to control specimens' temperature. As fatigue is a time-depended and long-lasting procedure, tests lasted for more than two weeks. Figure 8 shows a snapshot of the interface used to define the control parameters such as the minimum and maximum forces, along with the respective displacement values. The force and displacement values are shown in real time (in the form of a sinus equation).

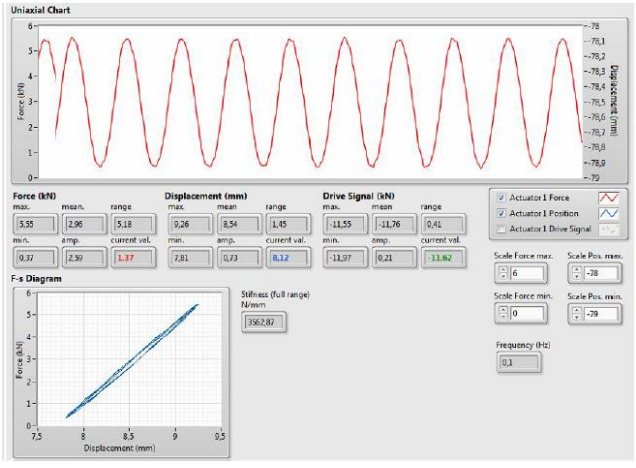

Fig. 8. The interface used to setup the fatigue experiments

The loading stress ratio was set at R=0, meaning that the specimens were loaded only from 0 up to a pre-specified stress. According to Table 1, fatigue specimens were of the same geometry as those printed for the tensile testing.

3. RESULTS AND DISCUSSIONS

3.1 Tensile

In Figure 9, the stress-strain graph of the PLA-v specimen is shown and in Figure 10 the stress-strain graphs of the PLA specimens are provided. Based on the graphs, an orthotropic behavior for PLA was observed; PLA-v specimen, that was built vertically, showed an ultimate tensile strength (UTS) ofσ_{max}=14MPa, whereas PLA specimens built horizontally showed an UTS of σ_{max}=42.4MPa. According to Figure 10, PLA shows a plastic deformation. The mechanical properties for tension are collected in Table 2, where σ_{max} is the ultimate tensile strength (UTS), σ_y is the yield tensile strength, σ_{break} is the tensile break strength, $\varepsilon_{max,\ el}$ is the maximum elastic deformation, $\varepsilon_{max,\ pl}$ is the maximum plastic deformation ($\varepsilon_{max,\ el} + \varepsilon_{max,\ pl} = \varepsilon_{total}$), E is the Young's modulus, E_{max} is the maximum Young's modulus, F_{max} is the maximum force and A is the cross section area. Literature's values are also shown [25].

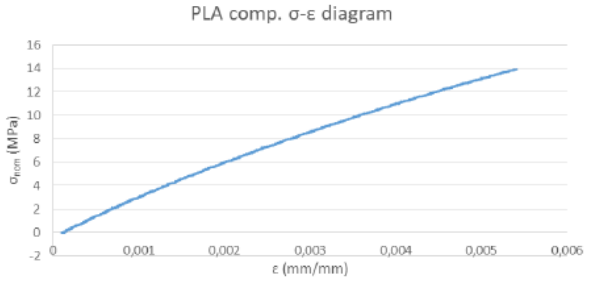

Fig. 9. Stress-strain diagram of the PLA comparison specimen

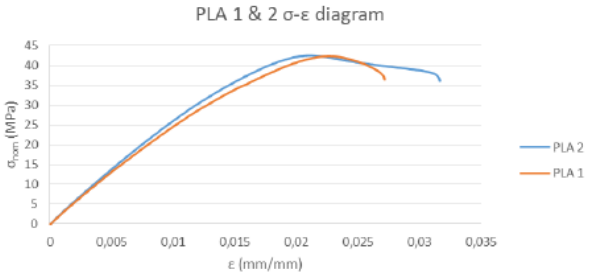

Fig. 10. Stress-strain diagrams of PLA specimens

Table 2. The tensile mechanical properties of the PLA specimens

	PLA-v	PLA 1	PLA 2	PLA average	Literature
σ_{max} (MPa)	14	42.3	42.4	42.35	48-110
σ_y (MPa)	-	36.4	36	36.2	15.5-73
σ_{break}(MPa)	14	36.4	36	36.2	14-70
$\varepsilon_{max,\ el}$ (mm/mm)	0.0049	0.0162	0.0150	0.0156	-
$\varepsilon_{max,\ pl}$ (mm/mm)	-	0.0119	0.0174	0.01465	0.005-0.92
E (MPa)	2860	2609	2829	2719	2020-3550
E_{max} (MPa)	3060	2776	2961	2868.5	-
F_{max} (N)	200	724.2	708.1	716.15	-
A (mm^2)	14.31	17.12	16.68	16.90	-

The slightly lower value of σ_{max} compared with literature is attributed to the fact that the PLA spool used for the specimens was exposed to ambient atmosphere, which diminished its mechanical properties [26, 27].

Figure 11 shows the stress-strain diagrams during nylon tensile tests.Nylon specimens showed a plastic deformation with high energy absorption rate area created under the stress–strain curve. Due to high deformation, specimens failed exactly at the transition area, the location where the central layers of the material meet the clamping area, according to the manufacturing characteristics (Figure 12). The process is represented in Figure 13. Based on nylon's intrinsic characteristics the material can be elongated for up to 439% [20].

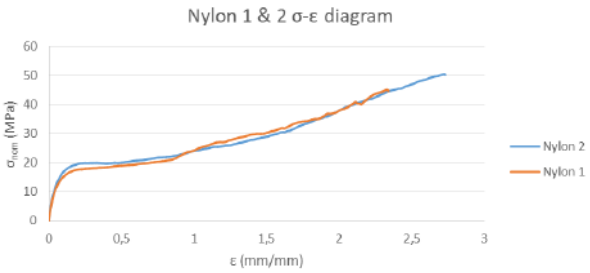

Fig. 11. Stress-strain diagrams of nylon specimens

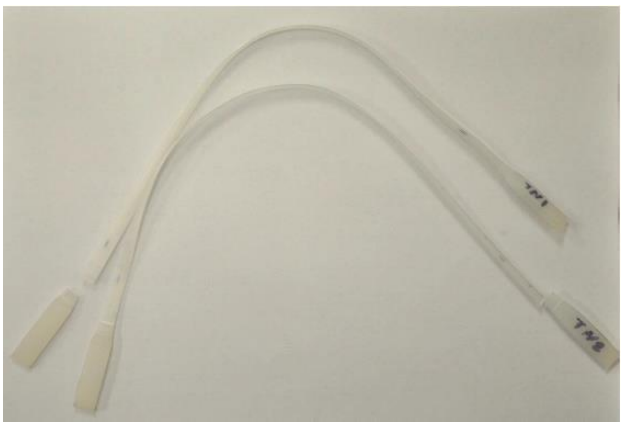

Fig. 12. The nylon specimens after tensile testing

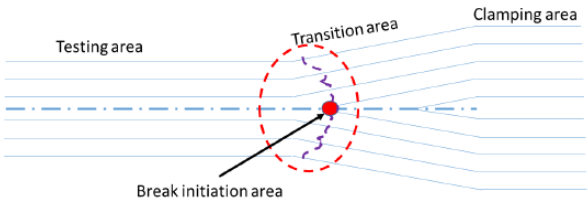

Fig. 13. Representation of the break initiation: light blue lines represent the edges of the material deposition

The mechanical characteristics of the nylon samples are collected in Table 3, where σ_{max} is the ultimate tensile strength (UTS), σ_y is the yield tensile strength,

σ_{break} is the tensile break strength, $\varepsilon_{max,\ el}$ is the maximum elastic deformation, $\varepsilon_{max,\ pl}$ is the maximum plastic deformation ($\varepsilon_{max,\ el} + \varepsilon_{max,\ pl} = \varepsilon_{total}$), E is the Young's modulus, E_{max} is the maximum Young's modulus, F_{max} is the maximum force and A is the cross section area. Literature's values are also shown [25].

Table 3. The tensile mechanical properties of the nylon specimens

	Nylon 1	Nylon 2	Nylon average	Literature
σ_{max} (MPa)	45.3	50.5	47.9	61
σ_y (MPa)	9.3	12.4	10.85	-
σ_{break} (MPa)	45.3	50.5	47.9	-
$\varepsilon_{max,\ el}$ (mm/mm)	0.136	0.148	0.142	-
$\varepsilon_{max,\ pl}$ (mm/mm)	2.204	2.587	2.3955	4.39
E (MPa)	332	342	337	530
E_{max} (MPa)	420	413	416.5	-
F_{max} (N)	727	816	771.5	-
A (mm^2)	16.064	16.13	16.097	-

In general, the main source of failure is attributed to geometric discontinuity or stress concentration. This form of discontinuity usually takes the form of a sharp change of geometry, opening, hole, notch, crack, etc. [28]. Classically, a notch-like defect can induce a crack when the stress field intensity near the notch root penetrates the process zone. In the current case, the lower values of tensile strength σ_{max} on the nylon 1-2 samples in comparison to the literature can be explained by the fact that the specimens failed near the clamping area due to the notch created by the printing process. The elastic modulus E differs also between nylon 1-2 samples and literature, which can be attributed to the plastic deformation and structural changes of material during processing.

During nylon testing, thecross-head speed (strain rate) plays a very crucial role in the process, as the material is highly elastic. In the ASTM standard used, the specification for the actuator movement is given in deformation rate of 2%/min. When calculated for the present specimens this is equal to 2mm/min. Other than that, nylon's behaviour was very interesting from real stresses point of view. When calculating the real cross section area where the specimen broke, the real stresses reached 102 and 153MPa for nylon 1 and nylon 2 samples, respectively. This means that the nylon is suitable for high elongation applications like under impact forces.

The nylon-carbon samples showed an average tensile strength of 923MPa. Figure 14 represents the stress-strain graphs of the samples while Figure 15 shows the samples after testing. An almost linear evolution can be observed until reaching the failure load. Usually an explosive failure could be expected, due to the alignment of the fibre with the load. Nevertheless, according to Figure 15, the failure occurred with a break almost perpendicular to the loading direction. This implies the presence of internal defects in the printed parts. Pressure during printing plays a critical role on the properties of both thermoset and thermoplastic based composites. The absence ofpressureis related to the presence ofdefects (pores and large matrix-dominated zones). Furthermore, the use ofinjector during printing may lead to thewavinesseffect on the fibres [29, 30].

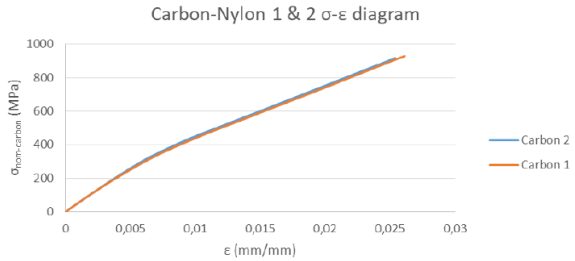

Fig. 14. Stress-strain graphs of nylon-carbon samples

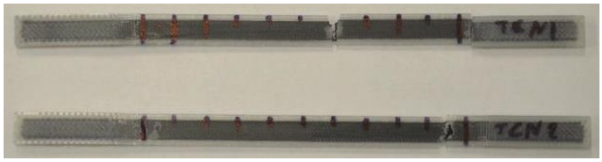

Fig. 15. The nylon-carbon samples after testing

The elastic deformation of the nylon-carbon samples is attributed to the carbon fibers. Young's modulus value was found to be like that provided by literature for nylon-carbon. Tensile strength of 986MPa was previously reported for CFF samples. Usually, early fibre fracture of possibly wrinkled fibres, followed by relaxation of most of the fibres leading to a better alignment at higher load levels, is observed during testing [12].

The resulted mechanical properties for tension of the nylon-carbon samples are collected in Table 4, where σ_{max} is the ultimate tensile strength (UTS), σ_y is the yield tensile strength, σ_{break} is the tensile break strength, σ_{nom} is the UTS for nominal cross section area, $\varepsilon_{max,\ el}$ is the maximum elastic deformation, $\varepsilon_{max,\ pl}$ is the maximum plastic deformation ($\varepsilon_{max,\ el} + \varepsilon_{max,\ pl} = \varepsilon_{total}$), E is the Young's modulus, E_{max} is the maximum Young's modulus, F_{max} is the maximum force, A is the cross section area and A_{nom} is the nominal cross section area. Literature's values are also shown [25].

Table 4. The tensile mechanical properties of the nylon-carbon specimens

	Nylon-carbon 1	Nylon-carbon 2	Nylon-carbon average	Literature
σ_{max} (MPa)	929.2	917.0513	923.1256	700
σ_y (MPa)	-	-	-	-
σ_{break} (MPa)	929.2	917.0513	923.1256	700
σ_{nom} (MPa)	226.5	223.5	225	-
$\varepsilon_{max,\ el}$ (mm/mm)	0.0177	0.0175	0.0176	0.012
$\varepsilon_{max,\ pl}$ (mm/mm)	0.031	0.0306	0.0308	0.015
E (MPa)	52460.25	53249.93	52855.09	54000

E_{max} (MPa)	54767.43	55055.61	54911.52	-
F_{max} (N)	3623.9	3576.5	3600.2	-
A (mm^2)	3.9	3.9	3.9	-
A_{nom} (mm^2)	16	16	16	-

3.2 Fatigue

There are many types of fatigue like mechanical, thermal and chemical and the mechanism behind is the weakening of a material structure, in which cracks grow under repeatedly applied loads [31]. The results of fatigue testing are usually represented as stress-life (S-N) curves also known as Wöhler curves [32, 33]. There are three areas on this type of graphs: a) the low cycle fatigue that stress amplitude is almost as high as the materials tensile strength, b) the normal fatigue area, that designers use to give dimensions to the lightweight and more sophisticated designs like airplane components, and finally c) the high cycle fatigue area, used for components that are meant to last for more than one lifetime, this area is beneath the fatigue strength limit.

The higher the stress, the smaller the number of cycles before failure. For some materials the S–N curve becomes horizontal at higher number of cycles.Below this stress level, fatigue failure will not occur. Some other materials do not have a fatigue limitandthe S–N curve continues its downward trend at increasingly greater number of cycles. For these materials, the fatigue response is specified as fatigue strength, which is defined as the stress level at which failure will occur for some specified number of cycles [31].

The testing stress levels are set strategically having in mind the total duration of the experiment series. Four levels were tested. The highest level was at 89% of the UTS, the second 84%, the third 81% and the fourth 78%. In Table 5 the samples tested during fatigue are shown with the respective stress amplitude for R=0. Each specimen was tested by controlling the stress values from the strain gages.

Table 5. Fatigue specimens (No 5-9) and results. Where R is the loading stress ratio, N the number of cycles and σ_{max} the maximum stress

Speciment No. for R=0	N	σ_{max} (MPa)
7	401	821
6	468	821
8	58683	769
5	238041	744
9	292722	718

Figure 16 shows a load sequence during testing, where the graph of stress versus time reveals the values needed for the fatigue calculations: the minimum, σ_{min}=11MPa and the maximum, σ_{max}=718MPa stress (sample No 9).

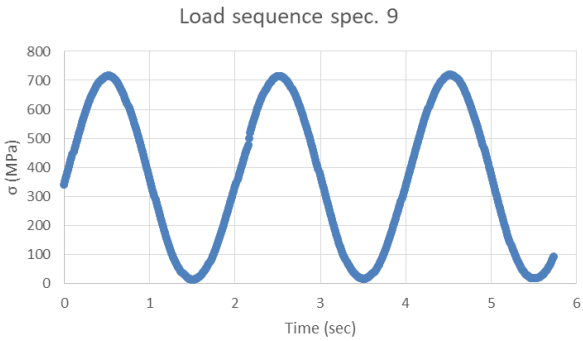

Fig. 16. Load sequence of specimen 9during fatigue test

All specimens failed near the clamping area and inside the controlled area with no signs of delamination in the breakage area, showing good adhesion between nylon and carbon. An example of sample breakage is shown in Figure 17.

Fig. 17. Specimen after fatigue test

Despite the fact that the number of experiments is small, some basic knowledge on the specimens fatigue characteristics can be gained.

Based on the results above, the S-N curve (a trend line) can be calculatedby transferring data into logarithmic scale. After calculating the mid-pointas an average of the logarithms, σ_{mean}=774MPa and N_{mean}=15032 and the slope of the trend line (linear regression), k=53.5, the inference of an almost flat slope can be drawn when comparing the calculated slope value to the steel's k, ranging usually from 4 to 8. This is a behavior that carbon fibres exhibit as they are relatively fatigue insensitive [32], having an almost flat slope.The S-N graph resulted is shown in Figure 18.

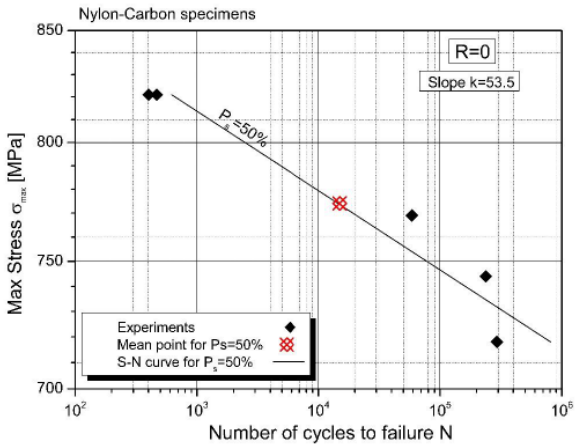

Fig. 18. The S-N curve with probability of survival, P_s=50% (scatter band, TN=8.75)

The curve shown in Figure 18 represents the specimen's S-N curve with a P_s=50% probability of survival. Therefore, high maximum stress values of above 700MPa can be achieved for fatigue life of 10^6 cycles, which would allow manufacturers design special lightweight structures with advanced mechanical properties.For instance, an N=10^7 cycles to failure component could have a maximum stress level of 685MPa for R=0 and a probability of survival, P_s=50%.

In the design guidelines, like FKM Guideline [33], the rules are applied for long lasting components, the fatigue strength is set as the load level that failure occurs in 10^6, or 10^7 depending on the component characteristics and nature, with a probability of survival P_s=97.7%. Despite the small number of experiments, it could be calculated that for P_s=97.7% and N=10^7 the fatigue strength is 664MPa, which is still very high and could be utilized for failure critical and long lasting lightweight components.

4. CONCLUSIONS

CFF can produce sophisticated and lightweight parts, while it can fully exploit the enhanced carbon fibers' rigidity and strength both in isotropic and concentric pattern even in fatigue conditions. The concentric pattern is more suitable for parts loaded axially or in bending and need strong outer surface. In the current work, the layers were adjusted to have the carbon fibres along the specimens, at 0deg, limiting the formation of a notch that could negatively affect specimen's tensile strength. The geometry used was designed in CAD software according to the dimensions given in ASTM D3039 and it was 3D printed with the isotropic fibre pattern configuration in order to induce only tensile stresses.

The testing results showed that the pure nylon specimens had plastic deformation behaviour with high energy absorption rate as seen from the area created under the tensile stress–strain curve in contrast to carbon fiber reinforced nylon, which had an almost elastic deformation behaviour. The modulus was significantly increased from 337MPa to 53000MPa, while the strength was increased from 48MPa to 923MPa since the specimen fully utilized the carbon fiber strength with a great level of adhesion between nylon and the carbon fibers.

Even though more data is necessary for a full nylon-carbon fatigue model, a preliminary, critical though, S-N curve was fitted. Fatigue results when R=0 (unidirectional testing) showed that nylon did not play a crucial role to the specimens' fatigue life, serving only as the matrix in the composite specimen structure. Therefore, the carbon fibres in sensitiveness to such a loading regime can be also observed in this composite configuration.

Future investigation will include fatigue testing within a wider range of R-values and stress levels to better understand the mechanism behind failure. The results of the current work aim to contribute to the standardization of 3D printing production processes, since the derivation of the mechanical properties is the most crucial part in the optimization of materials and processes for the cost-efficient production of high-quality products.

5. REFERENCES

1. Achillas, C., Aidonis, D., Iakovou, E., Thymianidis, M., Tzetzis, D., (2015). *A Methodological Framework for the Inclusion of Modern Additive Manufacturing into the Production Portfolio of a Focused Factory*, Journal of Manufacturing Systems, **37**, 328–339.

2. Raimondo, M.O., Achillas, Ch., Tzetzis, D., (2017). *Alternative Business Strategies Based on the Comparison of Additive and Traditional Manufacturing Technologies*, International Journal of Production Research, **55**(12), 3497–3509.

3. Mansour, M., Tsongas, K., Tzetzis, D., (2019). *Measurement of the mechanical and dynamic properties of 3D printed polylactic acid reinforced with graphene*, Polymer-Plastics Technology and Materials, **58**(11),1234-1244.

4. Kyratsis, P., Tzetzis, D., (2018). *Investigation of the Mechanical Properties of Acrylonitrile Butadiene Styrene (ABS)-Nanosilica Reinforced Nanocomposites for Fused Filament Fabrication 3D Printing*, IOP Conference Series: Materials Science and Engineering, **416**(1), 012086.

5. Gioumouxouzis, C.I., Baklavaridis, A., Katsamenis, O.L., Markopoulou, C.K., Bouropoulos, N., Tzetzis, D., Fatouros, D.G., (2018).*A 3D Printed Bilayer Oral Solid Dosage Form Combining Metformin for Prolonged and Glimepiride for Immediate Drug Delivery*, European Journal of Pharmaceutical Sciences, **120**, 40–52.

6. Gioumouxouzis, C.I., Chatzitaki, K., Karavasili, C., Katsamenis, O.L., Tzetzis, D., Bouropoulos, N., Fatouros, D.G., (2018). *Controlled Release of 5-Fluorouracil from Alginate Beads Encapsulated in 3D Printed pH-Responsive Solid Dosage Forms*, AAPS PharmSciTech, **19**(8), 3362-3375.

7. Fragkos, S., Tzimtzimis, E., Tzetzis, D., Dodun, O., Kyratsis, P., (2018). *3D laser scanning and digital restoration of an archaeological find*, MATEC Web of Conferences, **178**, 03013.

8. Efstathiadis, A., Koidis, C., Tzetzis, D., Kyratsis, P., (2018). *Comparative study and analysis on the mechanical properties of 3D printed surgical instrument for in-space applications*, Academic Journal of Manufacturing Engineering, **16**(4), 26-32.

9. Rodriguez, J.F., Thomas, J.P., Renaud, J.E., (2000). *Characterization of the mesostructure of*

fused-deposition acrylonitrile-butadiene-styrene materials, Rapid Prototyp. J., **6**(3), 175–186.
10. Wu, W., Geng, P., Li, G., Zhao, D., Zhang, H., Zhao, J., (2015). *Influence of layer thickness and raster angle on the mechanical properties of 3D-printed PEEK and a comparative mechanical study between PEEK and ABS*, Materials (Basel), **8**(9), 5834–5846.
11. Huang, B., Singamneni, S., (2015). *Raster angle mechanics in fused deposition modelling*, J. Compos. Mater., **49**(3), 363–383.
12. Blok, L.G., Longana, M.L., Yu, H., Woods, B.K.S., (2018). *An investigation into 3D printing of fibre reinforced thermoplastic composites*, Addit. Manuf., **22**, 176–186.
13. Mansour, M., Tsongas, K., Tzetzis, D., Antoniadis, A., (2018). *Mechanical and Dynamic Behavior of Fused Filament Fabrication 3D Printed Polyethylene Terephthalate Glycol Reinforced with Carbon Fibers*, Polymer-Plastics Technology and Engineering, **57**,1715-1725.
14. Kousiatza, Ch., Tzetzis, D., Karalekas, D., (2019). *In-situ Characterization of 3D printed Continuous Fiber Reinforced Composites: A Methodological Study using Fiber Bragg Grating Sensors*, Composites Science and Technology, **174**, 134–141.
15. Prüß, H., Vietor, T., (2015). *Design for fiber-reinforced additive manufacturing*, J. Mech. Des., **137**(11), 111409.
16. Available from: https://markforged.com/, Accessed on: 14/04/2019.
17. ASTM E1823-13, (2013). *Standard terminology relating to fatigue and fracture testing*, ASTM International, West Conshohocken, 1034.
18. Stephens, R.I., Fatemi, A., Stephens, R.R., Fuchs, H.O., (2001). *Metal Fatigue in Engineering*, Second ed., Wiley, New York.
19. Dickson, A.N., Barry, J.N., McDonnell, K.A., Dowling, D.P., (2017). *Fabrication of continuous carbon, glass and Kevlar fibre reinforced polymer composites using additive manufacturing*, Addit. Manuf., **16**,146–152.
20. Kuchipudi, S.C., (2017). *The effects of fiber orientation and volume fraction of fiber on Mechanical properties of additively manufactured composite material*, All Theses, Dissertations, and Other Capstone Projects, 734, Minnesota State University.
21. Fischer, M., Schöppner, V., (2017). *Fatigue behavior of FDM parts manufactured with Ultem 9085*, JOM-J. Min. Met. Mat. S., **69**(3), 563–568.
22. Letcher T., Waytashek M., (2014). *Material property testing of 3D printed specimen in PLA on an entry-level 3D printer*, Proceedings of ASME 2014 International Mechanical Engineering Congress and Exposition, V02AT02A014, American Society of Mechanical Engineers, Montreal.
23. Imeri, A., Fidan, I., Allen, M., Wilson, D.A, Canfield, S., (2018). *Fatigue analysis of the fiber reinforced additively manufactured objects*, Int. J. Adv. Manuf. Technol., **98**, 2717–2724.
24. ASTM, (2016). *Annual book of ASTM standards*, American Society for Testing Materials International.
25. Lanzotti, A., Grasso, M., Staiano, G., Martorelli, M., (2015). *The impact of process parameters on mechanical properties of parts fabricated in PLA with an open-source 3-D printer*, Rapid Prototyp. J., **21**(5), 604–617.
26. Ho, K.-L.G., Pometto, A.L., Hinz, P.N., (1999). *Effects of temperature and relative humidity on polylactic acid plastic degradation*, J. Environ. Polym. Degr., **7**(2), 83–92.
27. Acioli-Moura, R., Sun, X.S., (2008). *Thermal degradation and physical aging of poly (lactic acid) and its blends with starch*, Polym. Eng. Sci., **48**(4), 829–836.
28. Mohammadi, S., (2008). *Extended Finite Element Method for Fracture Analysis of Structures*, Blackwell Publishing, Oxford, UK.
29. Justo, J., Távara, L., García-Guzmán, L., París, F., (2018). *Characterization of 3D printed long fibre reinforced composites*, Compos. Struct., **185**, 537–548.
30. Garnich, M.R., Karami, G., (2005). *Localized fiber waviness and implications for failure in unidirectional composites*, J. Compos. Mater., **39**(14), 1225–1245.
31. Wright, P., Fu, X., Sinclair, I., Spearing, S.M., (2008).*Ultra high resolution computed tomography of damage in notched carbon fiber–epoxy composites*, J. Compos. Mater., **42**(19), 1993–2002.
32. Campbell, F.C., (2012). *Fatigue and Fracture, Understanding the basics*, First ed., ASM International, Ohio.
33. FKM-Guideline, (2012). *Analytical Strength Assessment of Mechanical Components* – 6th Edition, VDMA Verlag, Frankfurt a.M.

Received: April 29, 2019 / Accepted: December 20, 2019 / Paper available online: December 25, 2019